

# Synergies between Unsaturated Zn/Cu Doping Sites in Carbon Dots Provide New Pathways for Photocatalytic Oxidation

Wenting Wu,<sup>†,§</sup> Qinggang Zhang,<sup>†</sup> Ruiqin Wang,<sup>†</sup> Yufei Zhao,<sup>‡</sup> Zhongtao Li,<sup>†</sup> Hui Ning,<sup>†</sup> Qingshan Zhao,<sup>†</sup> Gary P. Wiederrecht,<sup>\*,§</sup> Jieshan Qiu,<sup>\*,‡</sup> and Mingbo Wu<sup>\*,†,§</sup>

<sup>†</sup>State Key Laboratory of Heavy Oil Processing, College of Chemical Engineering, China University of Petroleum (East China), Qingdao 266580, P. R. China

<sup>‡</sup>State Key Lab of Fine Chemicals, School of Chemical Engineering, Dalian University of Technology, Dalian 116024, P. R. China

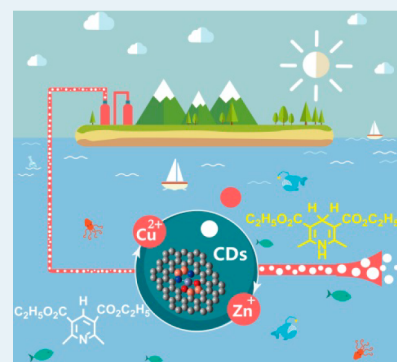
<sup>§</sup>Center for Nanoscale Materials, Argonne National Laboratory, Argonne, Illinois 60439, United States

<sup>‡</sup>Key Laboratory of Photochemical Conversion and Optoelectronic Materials, Technical Institute of Physics and Chemistry, Chinese Academy of Sciences, Beijing 100190, P. R. China

## Supporting Information

**ABSTRACT:** Unsaturated metal species (UMS) confined in nanomaterials play important roles for electron transfer in a wide range of catalytic reactions. However, the limited fabrication methods of UMS restrict their wider catalytic applications. Here, we report on the synergy of unsaturated Zn and Cu dopants confined in carbon dots (ZnCu-CDs) to produce enhanced electron transfer and photooxidation processes in the doped CDs. The Zn/Cu species chelate with the carbon matrix mainly through Cu–O(N)–Zn–O(N)–Cu complexes. Within this structure, Cu<sup>2+</sup> acts as a mild oxidizer that facilitates increases the unsaturated Zn content and also precisely tunes the unsaturated Zn valence state to Zn<sup>d+</sup>, where *d* is between 1 and 2, instead of Zn<sup>0</sup>. With the help of UMS, electron-transfer pathways are produced, enhancing both the electron-donating (7.0 times) and -accepting (5.3 times) abilities relative to conventional CDs. Because of these synergistic effects, the photocatalytic efficiency of CDs in photooxidation reactions is shown to improve more than 5-fold.

**KEYWORDS:** unsaturated Zn/Cu species, carbon dots, electron transfer, superoxide radical anion, photooxidation



## 1. INTRODUCTION

With relatively low valence, unsaturated metal species (UMS) show great potential for unique electron-transfer pathways of importance to photocatalysis due to the changes in electron configuration and valence state.<sup>1–7</sup> To our knowledge, only a few recent efforts have been devoted to the fabrication of UMS, especially for unsaturated Zn which until recently was not highly valued for catalysis. Furthermore, the value of UMS for facilitating photoinduced electron transfer and photocatalysis opportunities has not been fully explored due to stability issues. For example, unsaturated Zn<sup>d+</sup> (*d* < 2) can be obtained in the gas phase under harsh physical conditions.<sup>8–10</sup> However, the low synthesis yields and their high sensitivity to air or water hinder potential applications. Although Zn<sup>d+</sup> can be indirectly prepared through photoinduced electron transfer from zeolites to a Zn center,<sup>6,11</sup> the limited fabrication methods of UMS still restrict their wider applications in catalysis.<sup>12</sup> Therefore, it is highly desired to develop alternative and novel nanomaterials containing UMS and to carefully explore their roles in electron-transfer processes for photocatalysis.

When confined in carbon species, the incomplete reduction of high-valence metal complexes by nano carbon materials is a novel and facile approach to directly fabricate UMS. Carbon dots (CDs) with graphite conductive structure show unique

electronic properties that can potentially provide electron balance between UMS and carbon species, and ultimately stabilize the UMS.<sup>13</sup> Furthermore, the incorporation of another metal ion as a mild oxidant could finely tune the UMS's valence state by preventing over reduction into a zero-valence metal by carbon species. Limited success has been achieved in applying CDs to finely tune the valence state of UMS for catalysts, although the metal doped CDs on their catalytic activities have been recently reported.<sup>13,14</sup> In this work, we focused on creating unsaturated Zn species, which are difficult to prepare as described above, through the simultaneous use of Cu dopants. Cu is an excellent metal dopant for CDs to tune the Zn valence state because Cu is close to Zn in the periodic table of the elements and they have similar 3d and 4s electronic orbitals which benefit their electron exchange. Our approach is to pyrolyze ethylenediaminetetraacetic acid (EDTA) to form a graphite conductive structure in the presence of chelating Cu<sup>2+</sup> and Zn<sup>2+</sup> ions.<sup>13,15</sup> This further enables the reduction of Zn<sup>2+</sup> into Zn<sup>d+</sup> and subsequent electron transfer for photocatalysis opportunities. Therefore, Na<sub>2</sub>[Cu(EDTA)] and Na<sub>2</sub>[Zn-

**Received:** October 9, 2017

**Revised:** November 15, 2017

**Published:** December 7, 2017

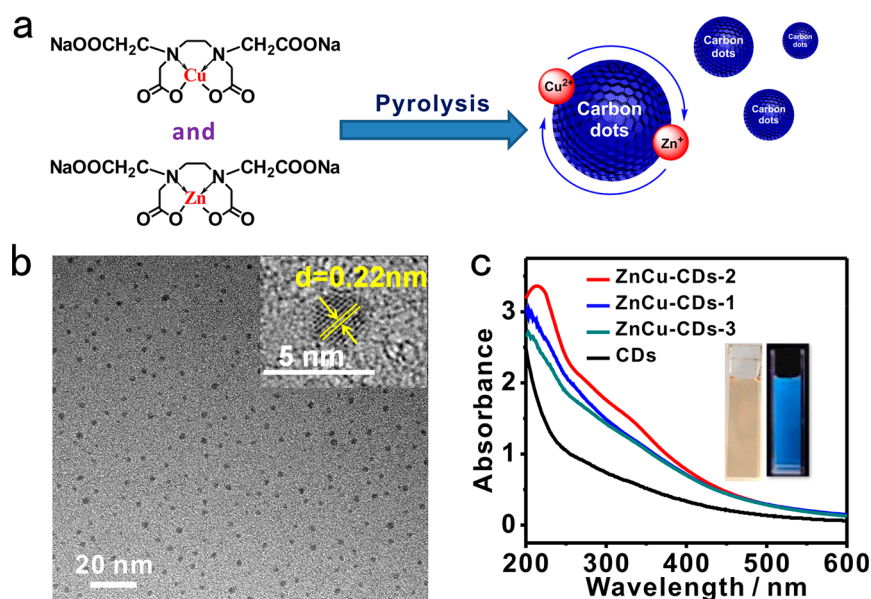


**Figure 1.** (a) Synthesis process of ZnCu-CDs. (b) TEM and HRTEM (inset) images of ZnCu-CDs-2. (c) UV-vis absorption spectra of ZnCu-CDs solution in deionized water,  $c = 0.15 \text{ mg}\cdot\text{mL}^{-1}$ . Inset: photographs of ZnCu-CDs-2 in daylight (left) and UV-light irradiation,  $\lambda_{\text{ex}} = 365 \text{ nm}$  (right).

(EDTA)] are good Cu and Zn precursors for the fabrication of Zn/Cu CDs.

Herein, CDs with unsaturated Zn/Cu species were prepared from the mixture of Na<sub>2</sub>[Cu(EDTA)] and diluted Na<sub>2</sub>[Zn(EDTA)] via a facile one-step pyrolysis. During pyrolysis, Zn<sup>2+</sup> was reduced into Zn<sup>d+</sup> ( $1 < d < 2$ ) species in the Zn/Cu-codoped carbon dots (ZnCu-CDs), which was confirmed by atomic absorption spectroscopy (AAS), electron spin resonance (ESR), TEM, XRD, Raman, X-ray photoelectron spectroscopy (XPS) and X-ray absorption fine structure (XAFS) spectroscopy. For Zn/Cu dopants in the graphene environment, their valence-state change can greatly enhance both the electron-donating/accepting abilities of the carbon dots, which were further confirmed by emission quenching tests and ESR. With an optimized mass ratio of Na<sub>2</sub>[Cu(EDTA)] and diluted Na<sub>2</sub>[Zn(EDTA)], ZnCu-CDs show extraordinarily high activity for the photooxidation of 1,4-dihydro-2,6-dimethylpyridine-3,5-dicarboxylate (DHP), which is the key component in various bioactive compounds and a good substrate for the production of pyridine derivatives.<sup>16,17</sup> Its conversion to diethyl 2,6-dimethylpyridine-3,5-dicarboxylate (DPy) is catalyzed by ZnCu-CDs at a rate 5 times higher than that of pure CDs.

## 2. EXPERIMENTAL SECTION

**2.1. Chemicals.** Ethylenediaminetetraacetic acid zinc disodium salt (Na<sub>2</sub>[Zn(EDTA)]), ethylenediaminetetraacetic acid copper disodium salt (Na<sub>2</sub>[Cu(EDTA)]), and ethylenediaminetetraacetic acid disodium salt (Na<sub>2</sub>[EDTA]) were purchased from Liaoyang Wan Rong Chemical Products Co., Ltd., China. All chemicals were directly used without further purification in our experiments.

**2.2. Synthesis of ZnCu-CDs.** A quartz boat filled with diluted-Zn-EDTA and Na<sub>2</sub>[Cu(EDTA)] (the mass ratio was 1:2, 1:1, and 2:1 for ZnCu-CDs-1, ZnCu-CDs-2, and ZnCu-CDs-3). The entire amounts of diluted-Zn-EDTA and Na<sub>2</sub>[Cu(EDTA)] (6 g) were thrust into the center of a quartz tube and calcined in a tube furnace at 350 °C for 2 h at a heating rate of 5 °C/min under N<sub>2</sub> atmosphere. The product was ground and dissolved in water (100 mL), and the

suspension was given a 300 W (40 kHz) ultrasonic treatment for 15 min at room temperature and then centrifuged at a high speed (10000 rpm) for 20 min. The upper brown solution was filtered with a slow-speed quantitative Millipore filter (0.22 μm) to remove the nonfluorescent deposited Na salts. After the filtering process, the solution was dialyzed with a MD34 (3500 Da) dialysis tube for 48 h to remove the remaining salts and small fragments. The concentrated solution was dried at 60 °C for 24 h, and CD powders were obtained. The amounts of each carbon dots obtained after purification were about 0.4–0.5 g. The CD powders can be soluble in ethanol/water mixed solvent.

**2.3. Photooxidation of DHP.** Photooxidation was carried out according to a modified literature method.<sup>13</sup> DHP, an organic substance, can be dissolved in some organic solvents (e.g., ethanol, methanol) better than in pure water. The CD powder can be hardly soluble in pure ethanol. Therefore, ethanol/water mixed solvent provides a homogeneous system containing CDs and DHP, which is beneficial to the catalytic reaction. An ethanol/water (1:1 v/v, 20 mL) mixed solvent containing DHP ( $1.0 \times 10^{-4} \text{ M}$ ) and the photosensitizer (CDs) was put into a two-neck round-bottom flask (50 mL). The solution was then irradiated using a xenon lamp with a power of about 35 W ( $600 \text{ W}\cdot\text{m}^{-2}$ ,  $\lambda$ : 385–800 nm) through a cutoff filter (0.72 M NaNO<sub>2</sub> solution, which is transmitted for light with  $\lambda > 385 \text{ nm}$ ). UV-vis absorption spectra were recorded at intervals of 2–5 min. The consumption of DHP was monitored by a decrease in the absorption at 374 nm, and the concentration of DHP was calculated by using its molar absorption coefficient ( $\epsilon = 7744 \text{ M}^{-1}\cdot\text{cm}^{-1}$ ). The photostability experiments were carried out by the same method without the substrate DHP (for the photosensitizers) or without photosensitizers (for DHP).

**2.4. Image and Spectroscopic Characterization.** Transmission electron micrographs (TEM) images were taken on a JEOL JEM-2100UHR microscope with an accelerating voltage of 200 kV. X-ray powder diffraction (XRD) was obtained by using PANalytical X-ray diffractometer equipped with Cu K $\alpha$  radiation ( $\lambda = 0.15406 \text{ nm}$ , 40 kV, 40 mA). Further evidence

for the composition of the product was inferred from X-ray photoelectron spectroscopy (XPS) using an ESCALAB 250Xi spectrometer equipped with source type (Al K Alpha). The depth of sampling the analytical information was 1–2 nm by Ar<sup>+</sup> ion bombardment. Raman spectroscopy was recorded using an Ar<sup>+</sup> ion laser at 514.5 nm wavelength (Renishaw in Via 2000 Raman microscope, Renishaw plc, UK) to assess the graphitic structure of raw materials and products. UV–vis absorption spectra were measured by a UV/vis spectrophotometer (Gold Spectrumlab 54, Shanghai Lengguang Technology Co., Ltd., China), and the concentrations of ZnCu-CDs solution in water were 0.15 mg·mL<sup>-1</sup>. Fluorescence spectra were measured by a spectrofluorometer (F-97 Pro, Shanghai Lengguang Technology Co., Ltd., China). Electron spin resonance (ESR) spectra were recorded using a JEOL JES FA200 spectrometer at 9.8 GHz, X-band, with 100 Hz field modulation. For the detection of superoxide radical anion, the solutions of CDs were quantitatively injected into specially made quartz capillaries for ESR analysis in the dark and illuminated directly in the cavity of the ESR spectrometer at room temperature. For the detection of Zn<sup>d+</sup> and Cu<sup>2+</sup>, the detector temperature was 77 K. Zn K-edge XAFS (X-ray absorption fine structure) spectra were collected at the beamline 1W1B with an Si (111) double-crystal monochromator at the Beijing Synchrotron Radiation Facility (BSRF). In all the test procedures, the samples (such as ZnCu-CDs, Na<sub>2</sub>[Zn(EDTA)], and ZnO) was sealed in 3 M tape and a plastic package. The XAFS data were analyzed using standard IFEFFIT procedures. All optical measurements were performed at room temperature.

**2.5. DFT Calculations.** To further confirm the structure and the total energy of UMS in ZnCu-CDs, theoretical studies were revealed by DFT calculations. Based on the extended EXAFS spectra for ZnCu-CDs-2, the four possible models are established by Gaussian 09 (Figure S8a–d). The ground-state geometries of the four models were optimized using DFT methods with a B3LYP/3-21G basis set. The total energies for the four models are shown in Table S3.

### 3. RESULTS AND DISCUSSION

To precisely fabricate UMS and finely tune their valence states, Na<sub>2</sub>[Zn(EDTA)] was first diluted by Na<sub>2</sub>(EDTA) with a mass ratio of 1:15, and the obtained mixture was named D-Zn-EDTA. The unsaturated Zn and Cu dopants were further balanced through thermolysis of the mixture of D-Zn-EDTA and Na<sub>2</sub>[Cu(EDTA)] at various ratios (1:2, 1:1, and 2:1 named ZnCu-CDs-1, ZnCu-CDs-2, and ZnCu-CDs-3, respectively) at 350 °C (Figure 1a). For CD samples with only Zn doping (Zn-CDs), the Zn content is 0.003 wt %, which is too low to improve the electron transfer (Table S1). For CD samples with only Cu doping (Cu-CDs), it is difficult to optimize the Cu valence state without the help of Zn (Figure S1a).<sup>13</sup> Furthermore, after centrifugation of the mixture containing ZnCu-CDs, the XRD of the precipitate shows that most of the metal species were reduced into metal (Cu<sup>0</sup>) by carbon (Figure S1b). To some extent, the reduction of Cu<sup>2+</sup> could prevent the over-reduction of Zn<sup>2+</sup>. The atomic absorption spectrum (Table S1) shows that the Zn content can go up to 0.15 wt % at a ratio of 1:1 (ZnCu-CDs-2). Compared with Zn-CDs, the Zn content is enhanced 50 times in ZnCu-CDs-2, which is also higher than those of other ratios (Table S1). In the following parts, ZnCu-CDs refers to the sample prepared with ratio of 1:1 at 350 °C. We also note that high-resolution Zn 2p and Cu 2p XPS spectra (Figure S2) show the presence of Zn (1021.8 and

1044.9 eV) and Cu (932.5 and 952.5 eV) in ZnCu-CDs.<sup>18,19</sup> After Ar<sup>+</sup> ion bombardment, the inner layers of ZnCu-CDs were exposed, but there is no obvious change in XPS spectra, indicating that the composition is very similar on the surface and inside the ZnCu-CDs.

TEM images of ZnCu-CDs clearly display uniformity with average diameters of 2.3 nm (Figure 1b and Figure S3a). The high-resolution TEM (HRTEM) image of the ZnCu-CDs clearly exhibits a good crystallinity of ZnCu-CDs with a lattice spacing of 0.22 nm corresponding to the lattice fringes of the (100) planes of graphite carbon, indicating that there are several layers of graphene in ZnCu-CDs.<sup>20–22</sup> This result is consistent with Raman spectroscopy (Figure S3b).<sup>23–25</sup> This graphene structure can benefit the electron exchange between the confined Cu and Zn sites for the photooxidation.

After Zn and Cu are confined in CDs, the visible-light-harvesting ability of ZnCu-CDs is greatly enhanced (Figure 1c). They show broadband absorption from 300 to 600 nm, which is much stronger than for pure CDs. It could be attributed to the coexistence of Cu/Zn dopants, producing metal-to-graphite charge-transfer (CT) absorption.<sup>13,26–28</sup> Interestingly, ZnCu-CDs-2 shows the strongest absorption intensity among these CDs, indicating that it may have the strongest electron exchange between Zn and Cu dopants at this ratio.<sup>29,30</sup> The color of the ZnCu-CD solution is brown under sunlight but gives blue emission when excited by 365 nm light (inset of Figure 1c). The further photoluminescent properties of ZnCu-CDs-2 are shown in Figure S4.<sup>25,31–33</sup> As the excitation wavelengths changes from 280 to 500 nm, the emission spectrum of ZnCu-CDs-2 exhibits a gradual red-shift phenomenon. The excitation-dependent PL behavior of the ZnCu-CDs-2 is similar to the CDs reported.<sup>34</sup> The excitation-dependent emission may be associated with the aromatic C=C bonds with various  $\pi$  conjugation and surface defects resulted from different groups (e.g., C–O) in the CDs.<sup>34–36</sup> After irradiation for 160 min, there is no obvious photobleaching for ZnCu-CDs-2, indicating that it is stable (Figure S5) and beneficial for their application in photocatalysis.<sup>13</sup>

The valence states of the Zn/Cu species confined in ZnCu-CDs were further investigated. ZnCu-CDs were measured by ESR spectroscopy at 77 K (Figure 2a). The Cu ESR spectroscopy (Figure 2a) shows that there is hyperfine structure at low fields, which can be assigned to the spin frustrated Cu<sup>2+</sup> dopant derived from the d orbital.<sup>37</sup> For Cu dopants, the *g* tensor parameter (*g*) of ZnCu-CDs is 2.06, indicating the covalent character of the Cu<sup>II</sup>–ligand bond inside the CDs.<sup>13,38</sup> The higher oxidation state and covalent character will produce greater electron-accepting character. The ESR signal of unsaturated Zn was also observed (Figure 2a). The *g* tensor parameter is 1.998, and the intensity and shape of the ESR signal is highly symmetrical. Thus, we assign this signal to the unpaired electron from the *s* orbital of Zn<sup>d+</sup> ( $0 < d < 2$ ), which is in good agreement with previous reports.<sup>6,11</sup> In order to further confirm this, the direct mixtures of CDs, Cu<sup>2+</sup>, and Zn<sup>2+</sup> salt were measured by ESR, and only a Cu<sup>2+</sup> signal was observed (Figure S6), indicating that the signal (*g* = 1.998) is not from precursors or carbon species. Furthermore, Cu-CDs were tested by ESR and show the same results (Figure S1a). ZnCu-CDs and Cu-CDs have similar precursors and were prepared under the same conditions. The only difference is the incorporation of Zn dopant. Thus, it indicates that this symmetrical signal (*g* = 1.998) is actually from Zn<sup>d+</sup> in the metal-doped CDs.

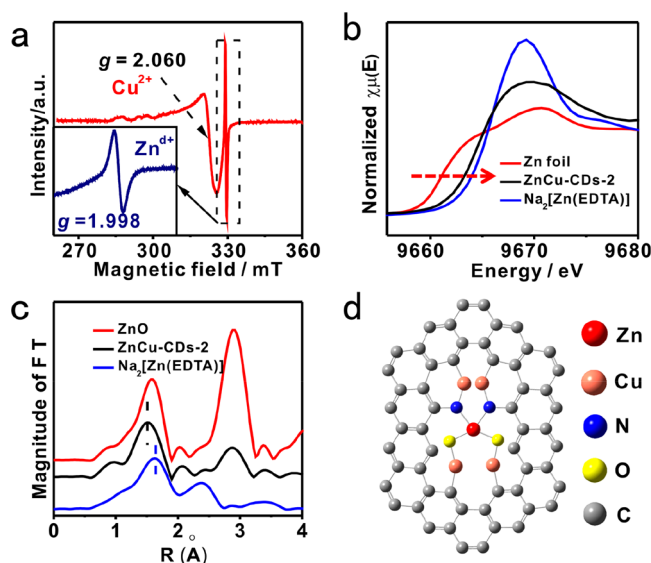


**Figure 2.** (a) ESR signal of  $\text{Cu}^{2+}$  from ZnCu-CDs-2. Inset: ESR signal of  $\text{Zn}^{2+}$  of ZnCu-CDs-2 at 77 K in the absence of oxygen. (b) Zn K-edge X-ray absorption near-edge structure (XANES) spectra of Zn foil,  $\text{Na}_2[\text{Zn}(\text{EDTA})]$ , and ZnCu-CDs-2. (c) EXAFS Zn K-edge radial distribution functions of ZnCu-CDs-2. (d) Structure model of an active metal dopant from ZnCu-CDs.

X-ray absorption fine structure (XAFS) spectroscopy is a powerful approach to further study the valence state, interatomic distance, and coordination number in CDs.<sup>7,39</sup> XAFS can be divided into two parts, X-ray absorption near edge structure (XANES) and extended X-ray absorption fine structure (EXAFS).<sup>40</sup> Generally, absorption edges shift to lower energies as the oxidation state is reduced.<sup>7</sup> The Zn K-edge absorption edge of ZnCu-CDs-2 is located between those of Zn foil and  $\text{Na}_2[\text{Zn}(\text{EDTA})]$  (Figure 2b). Combined with the unpaired electron from Zn ESR spectra, it is likely that the Zn species in ZnCu-CDs-2 has a lower average oxidation state ( $\text{Zn}^{d+}$ ,  $1 < d < 2$ ).<sup>6,7,40,41</sup> The Fourier transform of the Zn-extended EXAFS spectra for ZnCu-CDs-2 possesses two peaks probably corresponding to the Zn–O shell and Zn–O–Zn/Cu shells, respectively (Figure 2c). The first Zn–O shell has a distance of 1.97 Å and coordination number of 4.0, which is assigned to the Zn–O/N tetrahedron (Figure 2d). The average Zn–O/N distance is 1.97 Å, which is shorter than that of 2.10 Å observed for  $\text{Na}_2[\text{Zn}(\text{EDTA})]$  (Table S2).<sup>42</sup> In these metal-doped CDs, the copper content (0.73 wt %) is higher than zinc (0.15 wt %); thus, the second peak is probably from Zn–O–Zn/Cu, and mainly from Zn–O–Cu, which is also confirmed by the fitting results (Figure S7). In addition, DFT calculations were used to evaluate the total energy of UMS. Compared with other structures, Cu–O–Zn–N–Cu has the lowest energy (–291.0 keV, Figure S8 and Table S3). Therefore, the confinement structure of unsaturated Zn/Cu in CDs may be that the Zn/Cu species chelate with the carbon matrix mainly through Cu–O(N)–Zn–O(N)–Cu complexes. The average distance of Zn–O–Zn/Cu is 3.18 Å, shorter than Zn–O–Zn of ZnO (3.22 Å, Table S2). The shorter distance may benefit electron transfer between these metal dopants.

To investigate these metal-confinement performances, the photooxidation of DHP on CDs was characterized by UV/vis absorption spectra (Figure 3a and Figure S9),<sup>13</sup> which were irradiated under air instead of pure oxygen atmosphere. The product DPy was further confirmed by <sup>1</sup>HNMR and HRMS

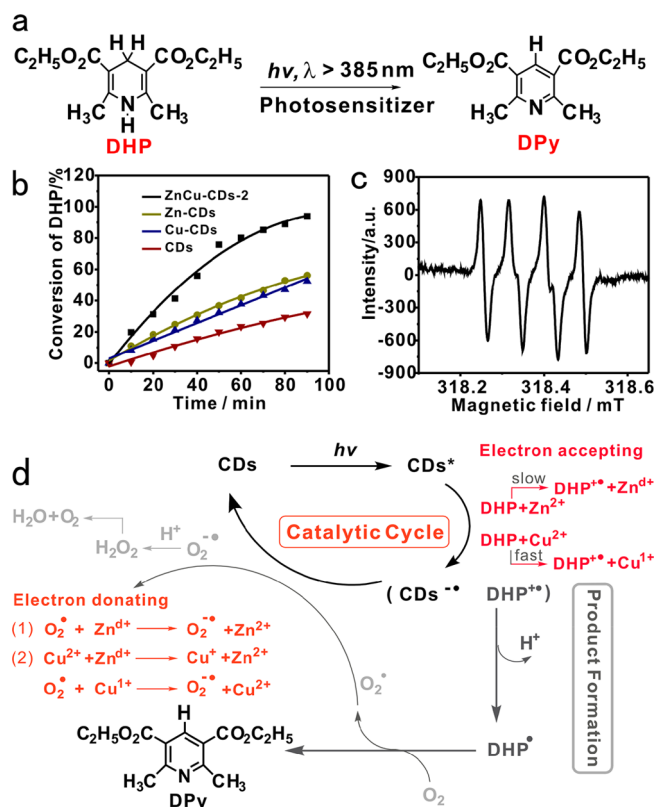


**Figure 3.** (a) Chemical equation for the photooxidation of DHP. (b) Conversion rate of DHP catalyzed by different CDs. (c) ESR signals of ZnCu-CDs-2 (1.5 mg/mL), DHP ( $1.0 \times 10^{-4}$  M), and DMPO ( $1.0 \times 10^{-2}$  M), irradiated for 15 min. (d) Mechanism for the photooxidation of DHP with superoxide radical anion ( $\text{O}_2^-$ ). The mechanism scheme could be divided into two parts: production formation and the catalytic cycle. For the product formation, the DHP easily lose an electron and subsequent  $\text{H}^+$  with the assistant of CDs, then  $\text{DHP}^\bullet$  transfer another electron to  $\text{O}_2$ , and obtained DPy, which are labeled in dark gray. For the catalytic cycle labeled in black, CDs play roles as both electron acceptor and donor, wherein the key electron transfer process with the assistant of unsaturated metal dopants or reactive oxygen species are highlighted in red. Detail descriptions are provided in the text and Supporting Information.

(Figures S10 and S11). For the pure CDs as photosensitizers, the conversion of DHP to DPy was only 31.6% after irradiation for 90 min. When doping with Zn/Cu species, the conversions after same irradiation for 90 min were significantly enhanced. For ZnCu-CDs-2, the conversion of DHP can go up to 93.9% (the conversion efficiency for all ZnCu-CDs is shown in Figure S12b). This conversion efficiency is also higher than others (Figure 3b, Figure S12, and Table S4). The photooxidation velocities of ZnCu-CDs were studied by plotting the  $\ln(A_t/A_0) - t$  curves (Figure S12a). The slope ( $k_{\text{obs}}$ ) of the photooxidation with ZnCu-CDs-2 is  $0.03 \text{ min}^{-1}$  (Table S4), which is 5 times higher than CDs. These results indicate that the incorporated Cu and Zn dopants can effectively enhance the CDs' photocatalytic efficiency.

It is noted that the electron transfer is crucial for the photooxidation.<sup>13,43,44</sup> The mechanism involving electron transfer is proposed and confirmed by ESR spectroscopy (Figure 3c,d and Figure S13).<sup>13,45</sup> The full description of the mechanism, involving electron transfer for the photooxidative aromatization of DHP catalyzed by ZnCu-CDs, is proposed in Figure 3d. First, CDs were photoexcited into the excited state

(CDs\*) and subsequent electron transfer from DHP (electron donor) to CDs\* (electron acceptor) produced the CDs\*<sup>-</sup> ( $\text{Zn}^{d+} \rightarrow \text{Zn}^{2+}$  and  $\text{Cu}^{2+} \rightarrow \text{Cu}^{1+}$ ) and DHP radical cation (DHP\*<sup>+</sup>). Then DHP\*<sup>+</sup> can release H<sup>+</sup> and its electron transfers to molecular oxygen under air atmosphere, generating DPY product. Subsequently, reactive oxygen radical ( $\text{O}_2^{\bullet}$ ) competes with the CDs\*<sup>-</sup> ( $\text{O}_2^{\bullet} + \text{Zn}^{d+} \rightarrow \text{O}_2^{\bullet-} + \text{Zn}^{2+}$ ,  $\text{O}_2^{\bullet} + \text{Cu}^{2+} \rightarrow \text{O}_2^{\bullet-} + \text{Cu}^{2+}$ ) to form superoxide anion radical ( $\text{O}_2^{\bullet-}$ ) and CDs anion restore the ground state. Finally,  $\text{O}_2^{\bullet-}$  reacts with H<sup>+</sup> to produce H<sub>2</sub>O<sub>2</sub>. H<sub>2</sub>O<sub>2</sub> is subsequently decomposed into O<sub>2</sub> and H<sub>2</sub>O with the help of CDs.

In order to confirm the electron-transfer mechanism, 5,5-dimethyl-1-pyrroline *N*-oxide (DMPO) was employed as scavenger for superoxide radical anion ( $\text{O}_2^{\bullet-}$ ). With the help of DMPO, the ESR signal attributed to  $\text{O}_2^{\bullet-}$  adduct was detected in the photoirradiation of ZnCu-CDs and substrate DHP. No such signal was detected in the absence of ZnCu-CDs or DHP (Figure S13). It indicates that electron transfer (DHP → ZnCu-CDs → O<sub>2</sub>) is crucial for the formation of  $\text{O}_2^{\bullet-}$ . During this photooxidation, the photosensitizer (ZnCu-CDs) switches its role from the electron acceptor to the electron donor. Their relative electron donating and accepting abilities were measured through emission quenching by the known electron acceptor 2,4-dinitrotoluene (DNT, -0.9 V vs NHE) and electron donor *N,N*-diethylaniline (DEA, 0.88 V vs NHE), respectively.<sup>22</sup> In Figure 4a,c,  $F_0$  stands for the original

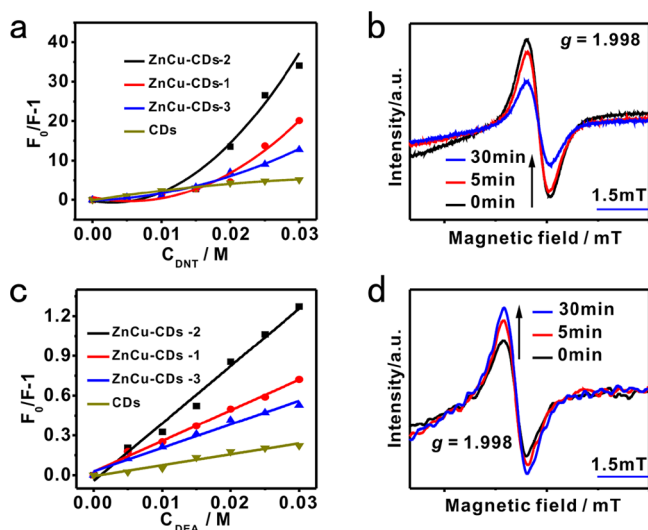


**Figure 4.** Assessment of electron-donating ability: (a) Stern–Volmer plot of the ZnCu-CDs emission intensity with various amounts of DNT in H<sub>2</sub>O ( $\lambda_{\text{ex}} = 350$  nm); (b) ESR signals of Zn<sup>2+</sup> of ZnCu-CDs (solid) without DHP, 77 K, in the absence of oxygen. Assessment of electron-accepting ability: (c) Stern–Volmer plot of the ZnCu-CDs emission intensity with various amounts of DEA in H<sub>2</sub>O ( $\lambda_{\text{ex}} = 350$  nm); (d) ESR signals of Zn<sup>2+</sup> of ZnCu-CDs with DHP, 77 K, in the absence of oxygen.

emission intensity of carbon dots, while  $F$  stands for the emission intensity of carbon dots with various amounts of DNT or DEA. The Stern–Volmer plots, in which the integrated emission intensity was plotted versus the quencher concentration (0–0.03M), assisted in analyzing the emission quenching (Figure 4).

For the electron-donating ability,<sup>46</sup> it is interesting that the Stern–Volmer plots show that the ZnCu-CDs all show nonlinear behavior as a function of DNT concentration (solid

lines are guides to the eye), while the pure CDs show linear behavior (Figure 4a and Figure S14). The Stern–Volmer quenching constant (slope) of ZnCu-CDs-2 was obviously larger than that of Zn-CDs, Cu-CDs, or CDs. This indicates that the doping of the dual-metal doped is beneficial to the photoluminescence quenching. With more Zn species (Figure 4a and Table S1), the upward-curve trend is obviously enhanced, indicating that there is a synergetic conversion between Zn and Cu species that aids the electron-donating ability of the ZnCu-CDs.<sup>47</sup> With the addition of DNT to 0.03M, the electron donating ability of ZnCu-CDs is 7 times that of CDs. When ZnCu-CDs were irradiated in the absence of oxygen, the ESR signal of both Cu<sup>2+</sup> (Figure S15a) and Zn<sup>d+</sup> (Figure 4b) became weak after irradiation for 30 min, and no other changes were detected. In addition, both Cu<sup>1+</sup> and Zn<sup>2+</sup> have no ESR signal and cannot be detected by ESR. This indicates that the conversions of Cu<sup>2+</sup> → Cu<sup>1+</sup> and Zn<sup>d+</sup> → Zn<sup>2+</sup> simultaneously occurred, e.g. the Cu<sup>2+</sup> was reduced by Zn<sup>d+</sup>.<sup>6</sup> It is a relatively slow process, and it is consistent with the emission quenching effect and the UV–vis absorption mentioned above (Figure 1c). Compared with that of the electron-accepting process, there is a more synergetic conversion between Zn and Cu species in the electron-donating process (vide infra). To some extent, it could reduce the recombination of electrons and holes and provide more efficient electron to the electron acceptor (e.g., DNT). Therefore, the assistance of Zn<sup>d+</sup> and subsequent conversions thus greatly enhances the electron-donating ability of ZnCu-CDs.

For the electron-accepting ability of CDs, the emission intensity was quenched with various DEA concentrations (Figure S16).<sup>22</sup> The Stern–Volmer quenching constants ( $K_{\text{SV}}$ ) for ZnCu-CDs-2 is 43.31 M<sup>-1</sup>, which is 5.3 times that of pure CDs (8.22 M<sup>-1</sup>) (Figure 4c). This quenching constant is also higher than Zn-CDs (9.70 M<sup>-1</sup>) and Cu-CDs (8.87 M<sup>-1</sup>) (Figure S16e). With increasing Zn content, the electron-accepting abilities of ZnCu-CDs also increase. Herein, the Stern–Volmer plots show a straight line, indicating that it may have only one active dopant. After addition of DHP, ESR signal of Cu<sup>2+</sup> from ZnCu-CDs sharply decreases and remains unchanged even after 30 min irradiation (Figure S15b), and it is a relative fast process. However, the ESR signal of Zn<sup>d+</sup> is enhanced during this process (Figure 4d). These results are consistent with quenching effect that only Zn<sup>d+</sup> participates in the photoinduced electron-accepting process on the time scale of the illumination. It is Zn<sup>d+</sup> that greatly enhances the electron-accepting ability.

Finally, electrochemical impedance spectroscopy (EIS) of different CDs was tested to assess the integral electron transfer ability (Figure S17). ZnCu-CDs-2 has the smaller diameter of Nyquist circle than Cu-CDs and CDs, further indicating that it has the lower charge-transfer resistance and that Zn actually enhances the electron transfer ability.

#### 4. CONCLUSION

In summary, ZnCu-CDs were prepared by one-step pyrolysis and show high catalytic activity for the photooxidation of DHP. XANES, ESR, and XPS provided clear evidence that Cu<sup>2+</sup> and carbon species help the formation of Zn<sup>d+</sup> species instead of Zn<sup>0</sup>. On the other hand, Zn<sup>d+</sup> can promote the Cu<sup>2+</sup> valence-state change (e.g.,  $\text{Zn}^{d+} + \text{Cu}^{2+} \rightarrow \text{Zn}^{2+} + \text{Cu}^{+}$ ) and provides unique electron-transfer pathways with the synergetic effect of Cu<sup>2+</sup> and graphene domains in carbon dots, enhancing both the

electron-donating/accepting abilities. Overall, this work not only provides an effective strategy for tuning the metal valence-state change but also expands the feasible applications of UMS with high catalytic activity, especially for efficient photo-oxidation and other solar-energy utilizations.

## ■ ASSOCIATED CONTENT

### Supporting Information

The Supporting Information is available free of charge on the ACS Publications website at DOI: 10.1021/acscatal.7b03423.

Additional characterization results and DFT calculation results (PDF)

## ■ AUTHOR INFORMATION

### Corresponding Authors

\*E-mail: wiederrecht@anl.gov.

\*E-mail: jqiu@dlut.edu.cn.

\*E-mail: wumb@upc.edu.cn.

### ORCID

Wenting Wu: 0000-0002-8380-7904

Jieshan Qiu: 0000-0002-6291-3791

Mingbo Wu: 0000-0003-0048-778X

### Notes

The authors declare no competing financial interest.

## ■ ACKNOWLEDGMENTS

This work was financially supported by NSFC (51672309, 21302224, 51172285 and 51372277) and the Fundamental Research Funds for Central Universities (15CX05010A, 14CX02127A, 15CX08005A). G.P.W. acknowledges support from the Center for Nanoscale Materials, a U.S. Department of Energy Office of Science User Facility under Contract No. DE-AC02-06CH11357. We also acknowledge fellowships from the China Scholarship Council (201706455027), the China Postdoctoral Science Foundation (2016M592268), and the Shandong Provincial Natural Science Foundation (ZR2016BB18).

## ■ REFERENCES

- (1) Ciamician, G. *Science* **1912**, *36*, 385–394.
- (2) König, B. *Chemical Photocatalysis*; De Gruyter: Berlin, 2013.
- (3) Hwang, Y. K.; Hong, D. Y.; Chang, J. S.; Jhung, S. H.; Seo, Y. K.; Kim, J.; Vimont, A.; Daturi, M.; Serre, C.; Férey, G. *Angew. Chem., Int. Ed.* **2008**, *47*, 4144–4148.
- (4) Horike, S.; Dinca, M.; Tamaki, K.; Long, J. R. *J. Am. Chem. Soc.* **2008**, *130*, 5854–5855.
- (5) Weng, Z.; Teo, S.; Koh, L. L.; Hor, T. *Angew. Chem., Int. Ed.* **2005**, *44*, 7560–7564.
- (6) Qi, G.; Xu, J.; Su, J.; Chen, J.; Wang, X.; Deng, F. *J. Am. Chem. Soc.* **2013**, *135*, 6762–6765.
- (7) Zhao, Y. F.; Chen, G. B.; Bian, T.; Zhou, C.; Waterhouse, G. I. N.; Wu, L. Z.; Tung, C. H.; Smith, L. J.; O'Hare, D.; Zhang, T. R. *Adv. Mater.* **2015**, *27*, 7824–7831.
- (8) Isoya, J. I.; Fujiwara, S. *Bull. Chem. Soc. Jpn.* **1972**, *45*, 2182–2188.
- (9) Rogers, W. T.; Stefani, G.; Camilloni, R.; Dunn, G. H.; Msezane, A. Z.; Henry, R. J. W. *Phys. Rev. A: At, Mol, Opt. Phys.* **1982**, *25*, 737–748.
- (10) Weis, P.; Kemper, P. R.; Bowers, M. T. *J. Phys. Chem. A* **1997**, *101*, 2809–2816.
- (11) Li, L.; Li, G. D.; Yan, C.; Mu, X. Y.; Pan, X. L.; Zou, X. X.; Wang, K. X.; Chen, J. S. *Angew. Chem.* **2011**, *123*, 8449–8453.
- (12) Fu, Qi.; Li, W. X.; Yao, Y. X.; Liu, H. Y.; Su, H. Y.; Ma, D.; Gu, X. K.; Chen, L. M.; Wang, Z.; Zhang, H.; Wang, B.; Bao, X. H. *Science* **2010**, *328*, 1141–1144.
- (13) Wu, W. T.; Zhan, L. Y.; Fan, W. Y.; Song, J. Z.; Li, X. M.; Li, Z. T.; Wang, R. Q.; Zhang, J. Q.; Zheng, J. T.; Wu, M. B.; Zeng, H. B. *Angew. Chem., Int. Ed.* **2015**, *54*, 6540–6544.
- (14) Zhang, Q. G.; Xu, W. M.; Han, C. C.; Wang, X. K.; Wang, Y. X.; Li, Z. T.; Wu, W. T.; Wu, M. B. *Carbon* **2018**, *126*, 128–134.
- (15) Ramanjaneya Reddy, G.; Balasubramanian, S.; Chennakesavulu, K. J. *Mater. Chem. A* **2014**, *2*, 15598–15610.
- (16) Zhang, D.; Wu, L. Z.; Zhou, L.; Han, X.; Yang, Q. Z.; Zhang, L. P.; Tung, C. H. *J. Am. Chem. Soc.* **2004**, *126*, 3440–3441.
- (17) Wang, D. H.; Liu, Q.; Chen, B.; Zhang, L. P.; Tung, C. H.; Wu, L. Z. *Chin. Sci. Bull.* **2010**, *55*, 2855–2858.
- (18) Chuai, Y. H.; Wang, X.; Shen, H. Z.; Li, Y. D.; Zheng, C. T.; Wang, Y. D. *J. Mater. Sci.* **2016**, *51*, 3592–3599.
- (19) Gayathri, P.; Senthil Kumar, A. *Langmuir* **2014**, *30*, 10513–10521.
- (20) Martindale, B. C.; Hutton, G. A.; Caputo, C. A.; Reisner, E. J. *Am. Chem. Soc.* **2015**, *137*, 6018–6025.
- (21) Huang, H.; Hu, H. L.; Qiao, S.; Bai, L.; Han, M. M.; Liu, Y.; Kang, Z. H. *Nanoscale* **2015**, *7*, 11321–11327.
- (22) Li, H. T.; Kang, Z. H.; Liu, Y.; Lee, S. T. *J. Mater. Chem.* **2012**, *22*, 24230–24253.
- (23) Liu, N.; Luo, F.; Wu, H. X.; Liu, Y. H.; Zhang, C.; Chen, J. *Adv. Funct. Mater.* **2008**, *18*, 1518–1525.
- (24) Li, Y.; Zhao, Y.; Cheng, H. H.; Hu, Y.; Shi, G. Q.; Dai, L. M.; Qu, L. T. *J. Am. Chem. Soc.* **2012**, *134*, 15–18.
- (25) Liu, R. H.; Huang, H.; Li, H. T.; Liu, Y.; Zhong, J.; Li, Y. Y.; Zhang, S.; Kang, Z. H. *ACS Catal.* **2014**, *4*, 328–336.
- (26) McCormick, T.; Jia, W. L.; Wang, S. *Inorg. Chem.* **2006**, *45*, 147–155.
- (27) Krylova, V. A.; Djurovich, P. I.; Aronson, J. W.; Haiges, R.; Whited, M. T.; Thompson, M. E. *Organometallics* **2012**, *31*, 7983–7993.
- (28) Golchoubian, H.; Rezaei, M. *Curr. Chem. Lett.* **2013**, *2*, 207–214.
- (29) Mohapatra, L.; Parida, K. *Catal. Sci. Technol.* **2017**, *7*, 2153–2164.
- (30) Sakuma, T.; Ohta, T.; Yagyu, T.; Takagi, H. D.; Inamo, M. *Inorg. Chem. Commun.* **2013**, *38*, 108–111.
- (31) Sun, Y. P.; Zhou, B.; Lin, Y.; Wang, W.; Fernando, K. A. S.; Pathak, P.; Meziani, M. J.; Harruff, B. A.; Wang, X.; Wang, H. F.; Luo, P. G.; Yang, H.; Kose, M. E.; Chen, B. L.; Veca, L. M.; Xie, S. Y. *J. Am. Chem. Soc.* **2006**, *128*, 7756–7757.
- (32) Sun, H.; Ren, J.; Qu, X. *Acc. Chem. Res.* **2016**, *49*, 461–470.
- (33) Zhao, A.; Chen, Z.; Zhao, C.; Gao, N.; Ren, J.; Qu, X. *Carbon* **2015**, *85*, 309–327.
- (34) Dong, Y.; Chen, C.; Lin, J.; Zhou, N.; Chi, Y.; Chen, G. *Carbon* **2013**, *56*, 12–17.
- (35) Wu, M.; Wang, Y.; Wu, W.; Hu, C.; Wang, X.; Zheng, J.; Li, Z.; Jiang, B.; Qiu, J. *Carbon* **2014**, *78*, 480–489.
- (36) Zhu, S.; Zhang, J.; Tang, S.; Qiao, C.; Wang, L.; Wang, H.; Liu, X.; Li, B.; Li, Y.; Yu, W.; Wang, X.; Sun, H.; Yang, B. *Adv. Funct. Mater.* **2012**, *22*, 4732–4740.
- (37) Nellutla, S.; van Tol, J.; Dalal, N. S.; Bi, L. H.; Kortz, U.; Keita, B.; Nadjjo, L.; Khitrov, G. A.; Marshall, A. G. *Inorg. Chem.* **2005**, *44*, 9795–9806.
- (38) Mohamed, T. A.; Shaaban, I. A.; Farag, R. S.; Zoghaib, W. M.; Afifi, M. S. *Spectrochim. Acta, Part A* **2015**, *135*, 417–427.
- (39) Bordiga, S.; Groppo, E.; Agostini, G.; van Bokhoven, J. A.; Lamberti, C. *Chem. Rev.* **2013**, *113*, 1736–1850.
- (40) Chen, G. B.; Zhao, Y. F.; Shang, L.; Waterhouse, G. I. N.; Kang, X.; Wu, L. Z.; Tung, C. H.; Zhang, T. R. *Adv. Sci.* **2016**, *3*, 1500424.
- (41) Xu, J.; Zheng, A. M.; Wang, X. M.; Qi, G. D.; Su, J.; Du, J. F.; Gan, Z. H.; Wu, J. F.; Wang, W.; Deng, F. *Chem. Sci.* **2012**, *3*, 2932–2940.
- (42) Schlegel, M. L.; Manceau, A.; Charlet, L. *J. Phys. IV* **1997**, *7*, 823–824.

(43) Zhang, J. Q.; An, X. H.; Lin, N.; Wu, W. T.; Wang, L. Z.; Li, Z. T.; Wang, R. Q.; Yang, W.; Liu, J. X.; Wu, M. B. *Carbon* **2016**, *100*, 450–455.

(44) Wu, W. T.; Zhang, J. Q.; Fan, W. Y.; Li, Z. T.; Wang, L. Z.; Li, X. M.; Wang, Y.; Wang, R. Q.; Zheng, J. T.; Wu, M. B.; Zeng, H. B. *ACS Catal.* **2016**, *6*, 3365–3371.

(45) Chen, F. Y.; Zhao, X.; Liu, H. J.; Qu, J. H. *Chem. Eng. J.* **2014**, *253*, 478–485.

(46) Wang, X.; Cao, L.; Lu, F.; Meziani, M. J.; Li, H.; Qi, G.; Zhou, B.; Harruff, B. A.; Kermarrec, F.; Sun, Y. P. *Chem. Commun.* **2009**, *46*, 3774–3776.

(47) Turro, N. J.; Ramamurthy, V.; Scaiano, J. C. *Modern Molecular Photochemistry of Organic Molecules*; University Science Books, Sausalito, CA, 2010; Vol. 8, pp 549–551.